González Suárez, A.; Trujillo Guillen, M.; Burdío, F.; Andaluz, A.; Berjano, E. (2014). Could the heat sink effect of blood flow inside large vessels protect the vessel wall from thermal damage during RF-assisted surgical resection?. Medical Physics. 41(8):083301-1-83301-13. doi:10.1118/1.4890103.

Could the heat sink effect of blood flow inside large vessels protect the vessel wall from thermal damage during RF-assisted surgical resection?

Ana González-Suárez[1], Macarena Trujillo[2], Fernando Burdío[3], Anna Andaluz[4], Enrique Berjano[1]

[1] *Biomedical Synergy, Electronic Engineering Department, Universitat Politècnica de València, Valencia, Spain*

[2] *Instituto Universitario de Matemática Pura y Aplicada, Universitat Politècnica de València, Valencia, Spain*

[3] *General Surgery Department, Hospital del Mar, Barcelona, Spain*

[4] *Departament de Medicina i Cirurgia Animals, Facultat de Veterinària, Universitat Autònoma de Barcelona, Barcelona, Spain*

*To whom all correspondence should be addressed:

Ana González Suárez

Electronic Engineering Department (7F)

Universitat Politècnica de València, Spain

Camino de Vera, 46022 Valencia, Spain

Email: angonsua@eln.upv.es

Purpose: To assess by means of computer simulations whether the heat sink effect inside a large vessel (portal vein) could protect the vessel wall from thermal damage close to an internally cooled electrode during RF-assisted resection.

Methods: Firstly in vivo experiments were conducted to validate the computational model by comparing the experimental and computational thermal lesion shapes created around the vessels. Computer simulations were then carried out to study the effect of different factors such as device-tissue contact, vessel position and vessel-device distance on temperature distributions and thermal lesion shapes near a large vessel, specifically the portal vein.

Results: The geometries of thermal lesions around the vessels in the in vivo experiments were in agreement with the computer results. The thermal lesion shape created around the portal vein was significantly modified by the heat sink effect in all the cases considered. Thermal damage to the portal vein wall was inversely related to the vessel-device distance. It was also more pronounced when the device-tissue contact surface was reduced or when the vessel was parallel to the device or perpendicular to its distal end (blade zone), the vessel wall being damaged at distances less than 4.25 mm.

Conclusions: Our computational findings suggest that the heat sink effect could protect the portal vein wall for distances equal to or greater than 5 mm, regardless of its position and distance with respect to the RF-based device.

Keywords: Blood flow, computer modeling, heat sink effect, in vivo model, large vessels, RF-assisted resection.

I. INTRODUCTION

Medical devices based on radiofrequency (RF) energy are usually employed during surgical resection to thermally coagulate medium and small vessels and consequently minimize intraoperative blood loss.[1] One of the most widely employed in clinical practice is the TissueLink dissecting sealer (Salient Surgical Technologies, Portsmouth, NH, USA), which is based on an irrigated electrode which infuses saline into the tissue through openings.[1] Other devices, such as the Coolinside device (Apeiron Medical, Valencia, Spain), are based on an internally cooled electrode.[2] In both devices, the electrode is cooled to prevent surface charring and keep the temperature on the device-tissue interface below 100ºC.[3] This allows deep thermal lesions to be created, which enhances the sealing of small and medium-sized vessels in the transection plane. However, the ability to create deep thermal lesions can become a drawback when the device is used in the proximity of large vessels. In this case, the surgeon needs to complete a transection plane near the large vessel without causing heat injuries to its wall. In fact, acute and delayed portal vein thrombosis as well as injury to the hepatic artery and bile duct have been observed following RF ablation near the liver hilum, which can lead to major morbidity such as bile stenosis and liver abscesses.[4,5] As a consequence, some surgeons prefer to substitute RF-based dissectors for ultrasonic dissectors when removing tissue around these large vessels in order to complete the transection plane and simultaneously to reduce the risk of thermal damage. The motivation is that ultrasonic dissectors have a low penetration depth and minimal lateral energy spread.[6]

In opposition to this idea, we hypothesize that the heat sink effect of the blood flow inside the large vessel could itself reduce thermal damage to its wall, i.e. RF-devices could be safely used under certain circumstances next to large vessels. To confirm this

hypothesis, we planned a computer modeling study. The first phase was to assess the validity of the computer model, and for this we conducted in vivo experiments in which the liver surface was heated by an internally cooled electrode placed as close as possible to a vessel with the aid of an ecograph. Only small and medium-sized vessels were found near the liver surface, since the large vessels (such as the portal vein) are located near the center of the organ and are thus less likely to be affected. The geometry and dimensions of the created thermal lesions were compared to those obtained from the computer simulations. Once the computational model was validated in this way, we conducted new computer simulations to assess the geometry and dimensions of the thermal lesions created by an internally cooled electrode near a large vessel, in this case the portal vein. We considered different relative positions and distances between the portal vein and the RF-based device. The results are expected to provide information on the importance of blood flow as a thermal protection mechanism, and to suggest a minimum safety distance between large vessels and an RF-based device.

II. MATERIALS AND METHODS

II.A. Description of the RF-assisted device

We considered an RF-based device based on an internally cooled 8 mm diameter Coolinside device (Apeiron Medical, Valencia, Spain), which is designed to coagulate and dissect hepatic parenchyma by a laparotomy approach.[2] Coagulation is performed by RF currents which are delivered to the tissue using any part of the electrode in contact with the tissue. The dissection is conducted using an 8 mm long blade attached to the distal tip of the electrode (see Figure 1).

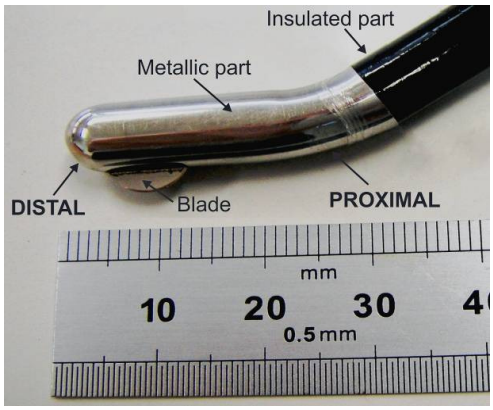

Figure 1 Coolinside device for RF-assisted resection (Apeiron Medical, Valencia, Spain). It is based on an internally cooled electrode 8 mm in diameter. The distal end is shown with the blade and proximal end joined to the insulated part of the device.

II.B. In vivo experimental set-up

The experimental procedure was approved by the Ethical Commission of the Universitat Autònoma de Barcelona (authorization numbers DAAM 6267 and CEEAH 1256). The in vivo experiments were conducted on one Landrace pig (weight 37.6 kg). Preoperative care and anesthesia were provided by fully trained veterinary staff. The animal was fasted for 12 hours before surgery. After initial sedation with a combination of azaperone and ketamine (4 and 10 mg kg^{-1} IM respectively), intravenous access was obtained through marginal ear-vein cannulation. Analgesia was provided with morphine (0.2 mg kg^{-1} IM) and anesthetic induction was performed with propofol (4 mg kg^{-1} IV). The animal was endotracheally intubated and anesthesia was maintained with isoflurane 2% in 100% oxygen. An infusion of lactated Ringer's solution was administered at a rate of 10 ml kg^{-1} h^{-1} during the entire study period. Heart rate, respiratory rate, pulse oximetry and capnography were monitored during anesthesia by a multiparametric monitor. Once anesthetized, the pig was positioned in dorsal recumbency and the abdomen was prepared aseptically. A midline laparotomy was performed and the liver was exposed. A high-resolution ultrasound system (Titan, SonoSite, Bothell, WS, USA)

was employed to measure the vessel diameter and the distance between the vessel and the treated area. A total of 6 thermal lesions were performed on the liver surface keeping the device totally placed over the tissue and perpendicular to the vessel. In the experiments a voltage[2] of 100 V for 45 s was applied using a CC-1 Cosman Coagulation System RF Generator (Radionics, Burlington, MA, USA). Finally, the animal was euthanized with pentobarbital sodium, immediately after which the liver was cut into 1 cm slices perpendicular to the applicator axis. The liver samples were stained with tetrazolium chloride (TTC)[7] to identify mitochondrial enzyme activity (i.e. viable cells) and were then macroscopically examined to evaluate the thermal lesion created around the vessels and to quantify any damage on the vessel wall. These lesions were characterized by a central "white zone" surrounded by a red hemorrhagic zone.[8] After staining with TTC, normal liver parenchyma and peripheral hemorrhagic zones were seen to be pink, but the central white zones were unstained since no viable cells were found.[7] The pink zones surrounding the central white zones were therefore excluded from the thermal lesions, since they consisted of non coagulated tissues (viable tissues).

II.C. Computer modeling

The theoretical model was based on a coupled electric-thermal problem, which was solved numerically using the Finite Element Method (FEM) with COMSOL Multiphysics software (COMSOL, Burlington, MA, USA). The governing equation for the thermal problem was the Bioheat Equation[9] which was modified by the enthalpy method[10,11] incorporating the phase change to model tissue vaporization:

$$\frac{\partial(\rho h)}{\partial t} = \nabla \cdot (k \nabla T) + q - Q_p + Q_m \qquad (1)$$

where ρ is density (kg m^{-3}), h enthalpy, t time (s), k thermal conductivity (W m^{-1}K^{-1}), T temperature (ºC), q the heat source caused by RF power (W m^{-3}), Q_p the heat loss

caused by blood perfusion (W m^{-3}) and Q_m the metabolic heat generation (W m^{-3}), which was considered negligible in comparison with the other terms.[12] In biological tissues enthalpy is related to tissue temperature by the following expression:[10,13]

$$\frac{\partial(\rho h)}{\partial t} = \frac{\partial T}{\partial t} * \begin{cases} \rho_l c_l & 0 < T \le 99^{\circ} C \\ h_{fg} C & 99 < T \le 100^{\circ} C \\ \rho_g c_g & T > 100^{\circ} C \end{cases} \quad (2)$$

where ρ_i and c_i is the tissue density and the specific heat of liver tissue before phase-change (i=l) and post-phase-change (i=g), respectively; h_{fg} is the latent heat and C the tissue water content. We considered a latent heat value of $2.162 \cdot 10^9$ J m^{-3}, which corresponds to the product of the water vaporization latent heat and the water density at 100ºC, and a tissue water content of 0.68 inside the liver tissue.[14]

The distributed heat sink effect of the microvascular perfusion was included in the tissue considering as:[9]

$$Q_p = \alpha \rho_b c_b \omega_b (T_b - T) \quad (3)$$

where ρ_b is blood density, c_b blood specific heat, T_b blood temperature (37ºC), α tissue state coefficient which ranges from 0–1, depending on the local level of tissue damage,[15,16] and ω_b blood perfusion coefficient (s^{-1}). In our study, the value of the blood perfusion coefficient in liver tissue was $\omega_b = 6.4 \cdot 10^{-3}$ s^{-1}.[17] The thermal damage of the tissue was assessed by the Arrhenius equation,[15,16] which associates temperature with exposure time using a first order kinetics relationship:

$$\Omega = \int_0^t A e^{\frac{-\Delta E}{RT}} dt \quad (4)$$

where Ω is the degree of tissue injury, R the universal gas constant, A the frequency factor (s^{-1}), and ΔE the activation energy for the irreversible damage reaction (J/mol). The parameters A and ΔE for the liver tissue were:[18] $A = 7.39 \cdot 10^{39}$ s^{-1} and ΔE =

$2.577 \cdot 10^5$ J mol^{-1}. We employed the thermal damage contour $\Omega = 1$, which represents 63% probability of cell death. When $\Omega > 1$, tissue coagulation is assumed to occur causing a cessation in tissue perfusion ($\alpha = 0$, $Q_p = 0$).[15]

The heat diffusion produced by the blood flow inside the vessel was simulated as a moving liquid[19] by including the so-called advection term[20] on the right of Eq. (1), which represents the heat loss due to blood flow:

$$-\rho_b c_b \mathbf{u}_b \cdot \nabla T \tag{5}$$

where $\mathbf{u}_b$ (x, y, z) is the blood velocity field in the vessel (m s^{-1}).

At the RF frequencies (≈500 kHz) and over the distance of interest, the biological medium can be considered almost totally resistive and a quasi-static approach is therefore possible to solve the electrical problem.[21] The distributed heat source q is given by $q = \sigma|\boldsymbol{E}|^2$, where $|\boldsymbol{E}|$ is the magnitude of the vector electric field (V m^{-1}) and σ is the electrical conductivity (S m^{-1}). $\boldsymbol{E}$ is calculated from $\boldsymbol{E} = -\nabla\Phi$, where Φ is the voltage (V) obtained by solving Laplace's equation:

$$\nabla \cdot (\sigma \nabla \Phi) = 0 \tag{6}$$

Figure 2 show the geometry and dimensions of the three-dimensional model. It represents a partially isolated metallic electrode in total contact with a fragment of hepatic tissue close to a vessel. The vessel with a diameter b and a length L (equal to the Y dimension of the tissue) is located perpendicular to and at distance (D) below the device. We initially modeled the same vessel diameters, vessel-device distances and vessel positions as those found in the experiments in order to validate the computational model. We considered a device insertion depth of 1 mm into the tissue due to the pressure of the electrode on the tissue. The physical dimensions of the device (Figure 2(b)) are those of the actual device shown in Figure 1: its metallic part is 30 mm long (L_M) and has outer and inner diameters of 8 and 7 mm, respectively (OD_M and ID_M).

The blade has a depth of 2.5 mm (P_B), being 0.1 mm thick (T_B) and 8 mm long (L_B); the plastic-covered section is 0.3 mm thick (T_P). In the model this plastic section is considered to be 45 mm long (L_P).

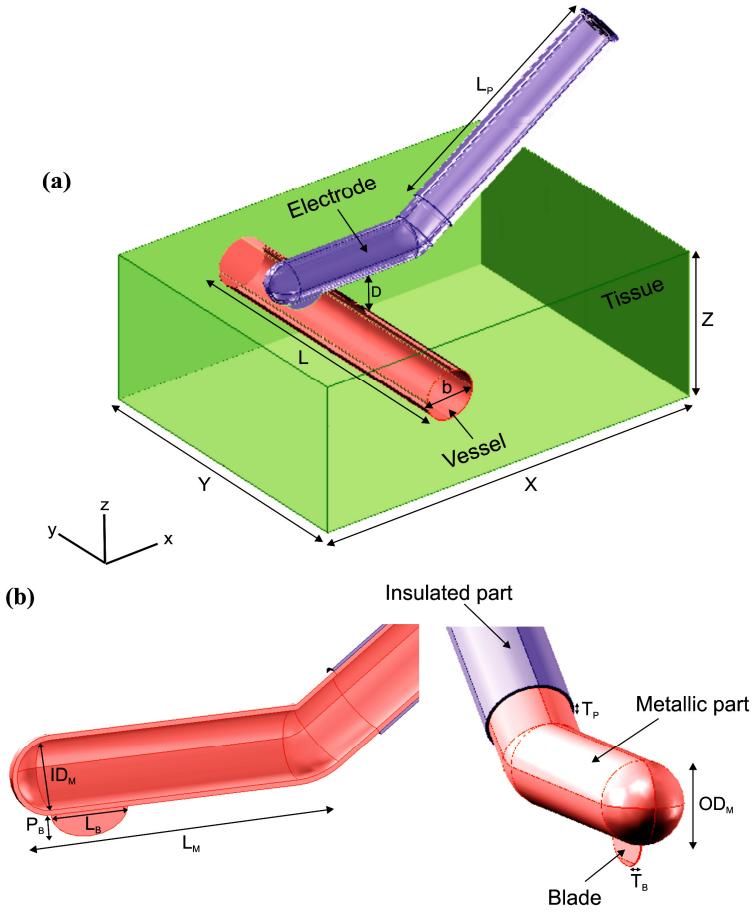

Figure 2 **(a)** Geometry and dimensions of the three-dimensional model built for the study. Tissue dimensions X, Y and Z (Z = Y/2) were obtained from a convergence test. The vessel, with a diameter b and a length L (L = Y), is located perpendicular to and at distance D below the electrode. L_P: length of the insulated section of the electrode. **(b)** Internal and external view and dimensions of the RF-assisted device. L_M: length of the metallic part in contact with the tissue; OD_M and ID_M: outer and inner diameter; P_B: insertion depth of the blade; L_B: blade length; T_B: blade thickness; T_P: thickness of the insulated section.

The appropriate tissue dimensions X = 80 mm, Y = 60 mm (Z = Y/2= 30 mm) were estimated by means of a convergence test in order to avoid boundary effects,[12] using as control parameter the value of the maximal temperature achieved in the tissue (T_{max})

after 45 s of RF heating. We first considered a tentative spatial (i.e. minimum meshing size) and temporal resolution. To determine the appropriate parameters of X and Y, we increased their values by equal amounts. When the difference in the T_{max} between consecutive simulations was less than 0.5%, we considered the former values to be adequate. We then determined adequate spatial and temporal resolution by means of similar convergence tests using the same control parameter. Discretization was spatially heterogeneous: the finest zone was always the blade-tissue interface, where the largest voltage gradient occurred and hence the maximum current density value. In the tissue, grid size was increased gradually with distance from the blade-tissue interface. In this regard, the convergence tests provided a grid size of 0.11 mm in the finest zone (blade-tissue interface) and a step time of 0.05 s. The model had nearly 80,000 tetrahedral elements.

The thermal and electrical properties of the model elements (electrode, plastic, blood and liver tissue) are shown in Table I.[14,22-25] The vessel wall was not modeled separately, since it has similar properties to normal liver tissue.[24] Liver electrical (σ) and thermal conductivity (k) were temperature-dependent and were defined by piecewise functions, Equations 7 and 8: for we considered an exponential growth[26] of 1.5%ºC^{-1} up to 100ºC, where 0.33 S m^{-1} was the value of the electrical conductivity assessed at 37ºC (see Table I), and then it decreased 4 orders for five degrees;[27] and k grew linearly 0.15%ºC^{-1} up to 100ºC, 0.502 W m^{-1} K^{-1} being the value of the thermal conductivity assessed at 37ºC (see Table I), after which k was kept constant.[11]

$$\sigma(T) = \begin{cases} 0.33e^{0.015(T-37)} & 0 < T \le 100^{\circ}C \\ 0.8490 - 0.1698 & 100 < T \le 105^{\circ}C \\ 0.8490 \cdot 10^{-4} & T > 105^{\circ}C \end{cases} \quad (7)$$

$$k(T) = \begin{cases} 0.502 + 0.015(T-37) & 0 < T \le 100^{\circ}C \\ 0.597 & T > 105^{\circ}C \end{cases} \quad (8)$$

Table I. Thermal and electrical characteristics of the elements employed in the numerical modeling (data from[14,22-25]): σ, electric conductivity; k, thermal conductivity; ρ, density; and c, specific heat.

Element/Material		σ (S m^{-1})	k (W m^{-1} K^{-1})	ρ (kg m^{-3})	c (J kg^{-1} K^{-1})
Electrode		$7.4 \cdot 10^{6}$	15	8000	480
Plastic		10^{-5}	0.026	70	1045
Blood		0.667	0.543	1000	4180
Liver tissue	Liquid phase	0.33*	0.502*	1080	3455
	Gas phase			370	2156

*Assessed at 37ºC.

Figure 3 shows the electrical and thermal boundary conditions applied to the model. For the electrical boundary conditions, a constant electrical voltage of 50 V was applied to the metallic part of the device and 0 V to the lower surface of the tissue (mimicking the electrical performance of the dispersive electrode). Although this voltage value is lower than that used in the in vivo experimental set-up, it should be remembered that the computational model (see Figure 2(a)) does not include the animal's entire body impedance, i.e. all impedance associated with the body and dispersive electrode,[28] and hence the voltage drop across the body and tissue next to the dispersive electrode is missing. Null electrical current was used on the surfaces at a distance from the device and on the tissue-ambient and device-ambient interfaces. For the thermal boundary conditions, a constant temperature of 37ºC was fixed on the surfaces at a distance from the device (this was also the initial temperature value). The effect of free convection at the tissue-ambient and device-ambient interfaces was taken into account using a thermal transfer coefficient (h_e) of 20 W m^{-2} K^{-1} and a value of 21ºC was considered for ambient temperature.[25] The cooling effect produced by the fluid circulating inside the device was not modeled realistically by means of internal tubes (the device was empty, as shown Figure 2(b)), but by a forced thermal convection coefficient (h_i) of 1420 W

m^{-2} K^{-1} and a coolant temperature of 5ºC. The value of this coefficient was estimated by using the theoretical calculation of forced convection inside a tube[25] with an inner diameter of 7 mm and a 30 mm length of heated area (ID_M and L_M in Figure 2(b), respectively). We considered an internal circulating fluid flow rate of 100 mL min^{-1} and half of the cross section area of the tube with a value of $1.92 \cdot 10^{-5}$ m^2.

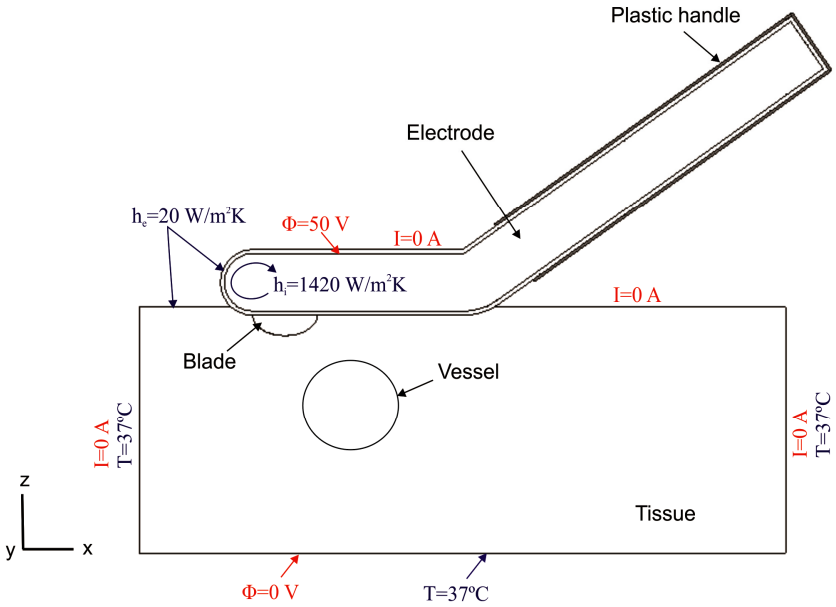

Figure 3 Electrical (red) and thermal (blue) boundary conditions of the computational model. The Figure shows the XZ-plane of the model.

II.D. Thermal modeling and damage quantification in the vessel wall

Once the computational model was validated, we conducted new simulations to study the effect of varying vessel-device distance, device-tissue contact and vessel-device position on the temperature distributions and thermal lesion shapes created around a large vessel. In this case we modeled the portal vein, with a diameter of 10 mm, which is its typical size at the liver hilum,[29] and a wall thickness of 0.5 mm.[30] Although some previous computer modeling studies[31,32] have considered vessel wall thickness (< 0.5 mm) as negligible when compared to its diameter, in our study it was crucial to consider this factor in order to assess whether the vessel wall had been damaged by RF heating.

We considered a blood flow velocity of 0.2 m s^{-1}, which is its typical average value in the portal vein.[33] We also increased this value from 0.2 to 0.8 m s^{-1} for one of the cases considered (specifically for the case of proximal device-tissue contact) in order to assess whether this parameter has an important effect on the thermal damage.

We modeled two relative positions of the device on the tissue: complete and proximal (only elbow zone) contact. Although in clinical practice the whole device is placed over the target tissue most of the time, i.e. its entire metallic length (L_M in Figure 2(b)) with the blade inserted in the tissue,[2] the surgeon can also choose to first treat the target tissue with the proximal part only (see Figure 1) to create a coagulation before placing the blade on the tissue.[34] In this case the contact surface is much smaller than in the case of total contact.

In the case of complete contact between device and tissue, we considered two relative vessel-device positions: perpendicular and parallel. With parallel vessel position, the portal vein was the same length as the tissue's dimension X. Regarding the perpendicular vessel position, we considered three relative positions of the vessel under the electrode: central, proximal and distal. In the case of proximal contact only, at an angle of 15º between electrode and tissue, we chose the worst case: i.e. with the vessel perpendicular to the device and below its point of contact. We also considered for each case different distances (D) from 1 to 5 mm between the device surface and the vessel wall. However, when the vessel was parallel to the device or perpendicular to its distal end, due to the presence of the blade, the distances range (D) was from 3.5 to 5 mm (i.e. leaving a gap of 1 mm between blade and vessel). In all the simulations an applied voltage of 50 V was considered for 45 seconds.[2] This time was considered long enough for the worst case, as surgeons rarely apply a device to a single point for a longer period.

The geometry of the thermal lesion around the portal vein after RF heating was obtained for each case. We proposed a new procedure to quantify the distances between the thermal lesion and the portal vein to assess whether its wall had been damaged by the RF heating. Only one previous study has measured the central distance between the RF lesion and the vessel.[22] In our study we not only quantified this distance, but also the transverse distances between the ends of the RF lesion and the vessel according to an angle θ, as well as some intermediate distances, as shown in Figure 4(a). These distances were then plotted on a graph according to the value of θ, to obtain the area under the curve between d_1 and d_9 (see Figure 4(b)). The thermal damage in the vessel wall was assessed by parameter β, which is the arc of the damaged vessel obtained by the intersection of the lesion curve with vessel wall thickness, as shown in Figure 4(b).

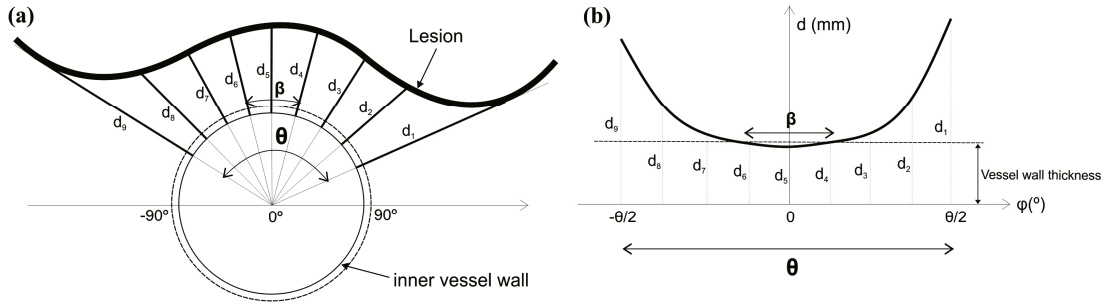

Figure 4 Procedure used to obtain the distances between the thermal lesion and the vessel in order to assess possible damage in the vessel wall: **(a)** Measurement of 9 distances according to angle θ, formed by the transverse distances between the lesion edges and the vessel (d_1 and d_9). **(b)** Graphical representation of these distances with respect to θ. The horizontal dashed line represents the vessel wall thickness and β the arc of the vessel damage.

III. RESULTS

III.A. Experimental validation

The vessels found in the experiments were small and medium-sized (see Figure 5(a)), with diameters ranging from 2.6 to 7.6 mm (4.05 ± 1.99 mm). It was extremely difficult

315 to find vessels very close to the device, and as shown in Figure 5(a) the distances between the device and the vessel (D) ranged from 7.4 to 16.2 mm (11.20 ± 3.98 mm). Figures 5(b) and (c) show the experimental and computational thermal lesions created around the vessels after 45 s of RF heating, which were assessed by the central "white zone" in the experiments and $\Omega = 1$ in the computer results. As can be seen, the 320 experimental and computational thermal lesion shapes created around the vessels were in close agreement, the walls not being damaged in any case. In addition, the experimental and computational thermal lesions also had similar lengths, which were 40.92 ± 1.65 and 41.10 ± 0.11 mm for the experimental and computational results. We did not compare the depth of either thermal lesion, since the in vivo scenario was 325 affected by the presence of other small vessels, as can be seen in Figure 5(b).

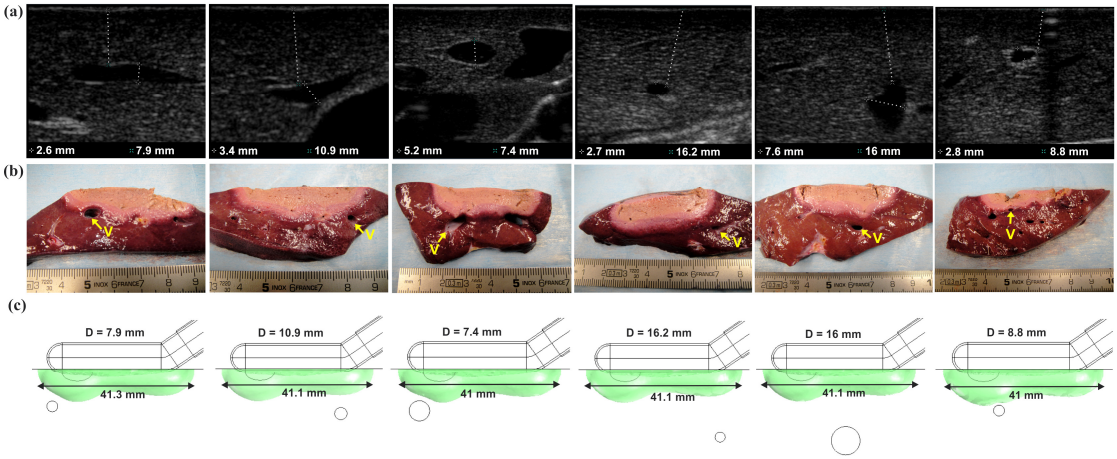

Figure 5 Sonography images **(a)** obtained from the experiments (n=6) where the vessel-device distance (D) and the vessel diameter were assessed. Experimental **(b)** and computational **(c)** thermal lesions created in the tissue after 45 s of RF heating with the whole device placed 330 on the tissue surface and the vessel perpendicular to the device at different distances (D) below it. "V" indicates the location of the vessel, whose diameter varies from 2.6 to 7.6 mm. The thermal damage surface corresponds to the "white zone" in the experimental results and to $\Omega = 1$ in the computer simulations. Note that the pink zones do not correspond to the thermal lesion, so that the "white zones" shown in **(b)** should be 335 compared to the corresponding computed lesion in **(c)**.

III.B. Thermal modeling and assessment of the thermal damage in the vessel wall

The evolution of the temperature distributions were plotted for the XZ-plane, which was oriented perpendicular to the blood vessel axis through the center of the model (see Figure 2(a)). Figure 6 shows the evolution of temperature distributions around the portal vein during 45 s of RF heating, considering total device-tissue contact, with the portal vein perpendicular to the device at a distance of 5 mm below its center. From the start (t = 5 s) heating was seen to be mainly located at the edges, especially around the tip of the blade and at the distal and proximal edges of the device. This edge effect was observed along the length of the device. A temperature of 100ºC was reached after 15 s at the proximal edge, where heating was even more intense than at the blade and proximal tip. The thermal lesion then moved towards the center of the tissue beneath the device (t = 25 s), where it reached a lower temperature (≈ 70ºC). After 45 s of RF heating the thermal damage had encircled the vessel leaving the wall intact.

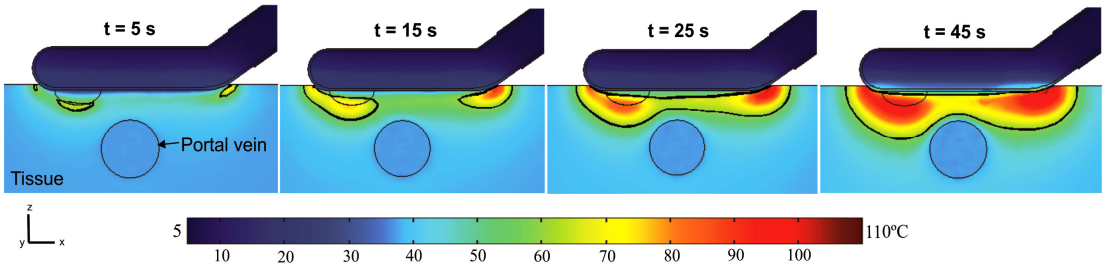

Figure 6 Evolution of the temperature distribution (in ºC) around the portal vein during RF heating, considering the device in total contact with the tissue and the portal vein perpendicular to the device and at a distance of 5 mm (D) below its center. The solid black line is the thermal damage border (Ω = 1).

Figure 7 shows the shapes of the thermal lesions created around the portal vein after 45 s of RF heating for different relative positions and distances between the portal vein and the device. The thermal lesions were plotted for the XZ-plane, as previously, and

also the YZ-plane, which was oriented perpendicular to the device's axis (see Figure 2(a)). The quantification of the distances between these thermal lesions and the portal vein used to assess thermal damage in the vessel wall are shown in Figure 8.

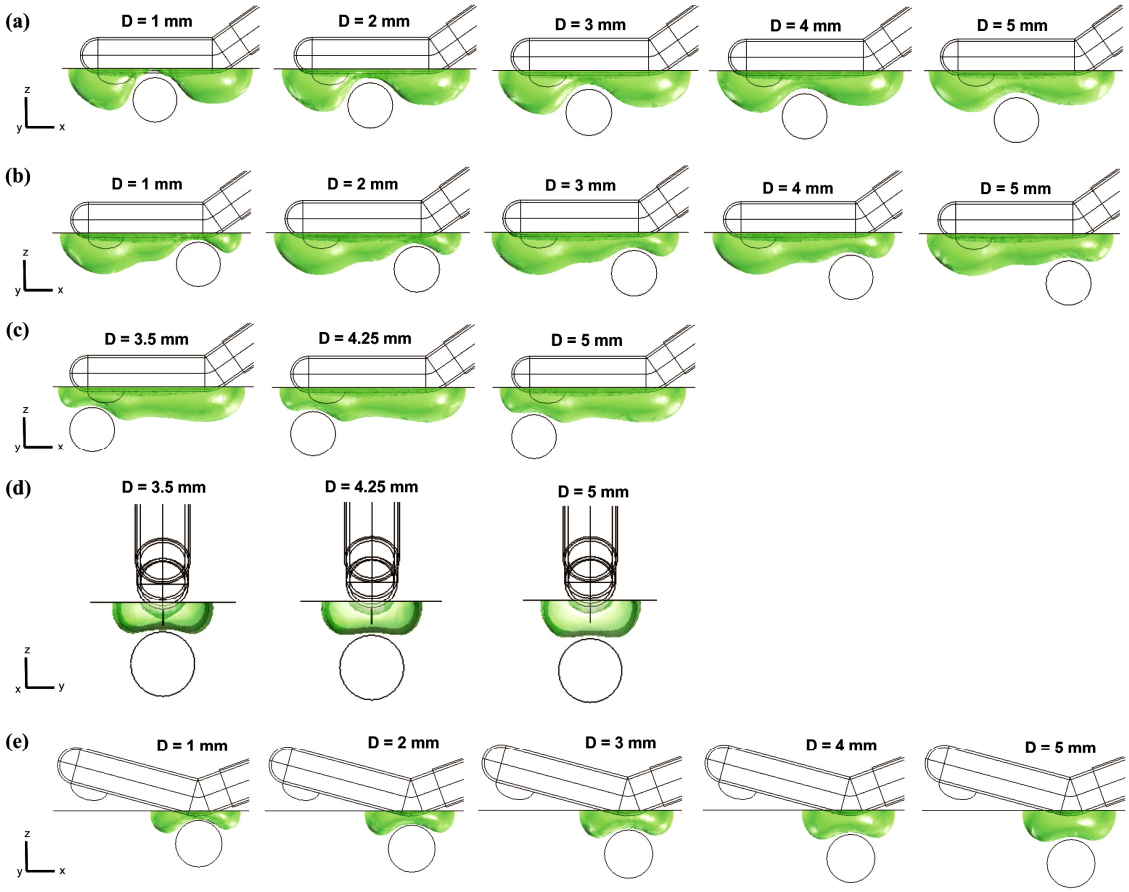

Figure 7 Thermal lesions created around the portal vein after 45 s of RF heating for different vessel-device distances (D), device-tissue contact conditions, and relative position of the vessel. Cases: total vessel-device contact and vessel perpendicular below the center of the device **(a)**, below its proximal end **(b)** and below its distal end **(c)**, vessel parallel to the device **(d)**, and only proximal vessel-device contact and vessel perpendicular to the device **(e)**. The thermal damage surface corresponds to $\Omega = 1$.

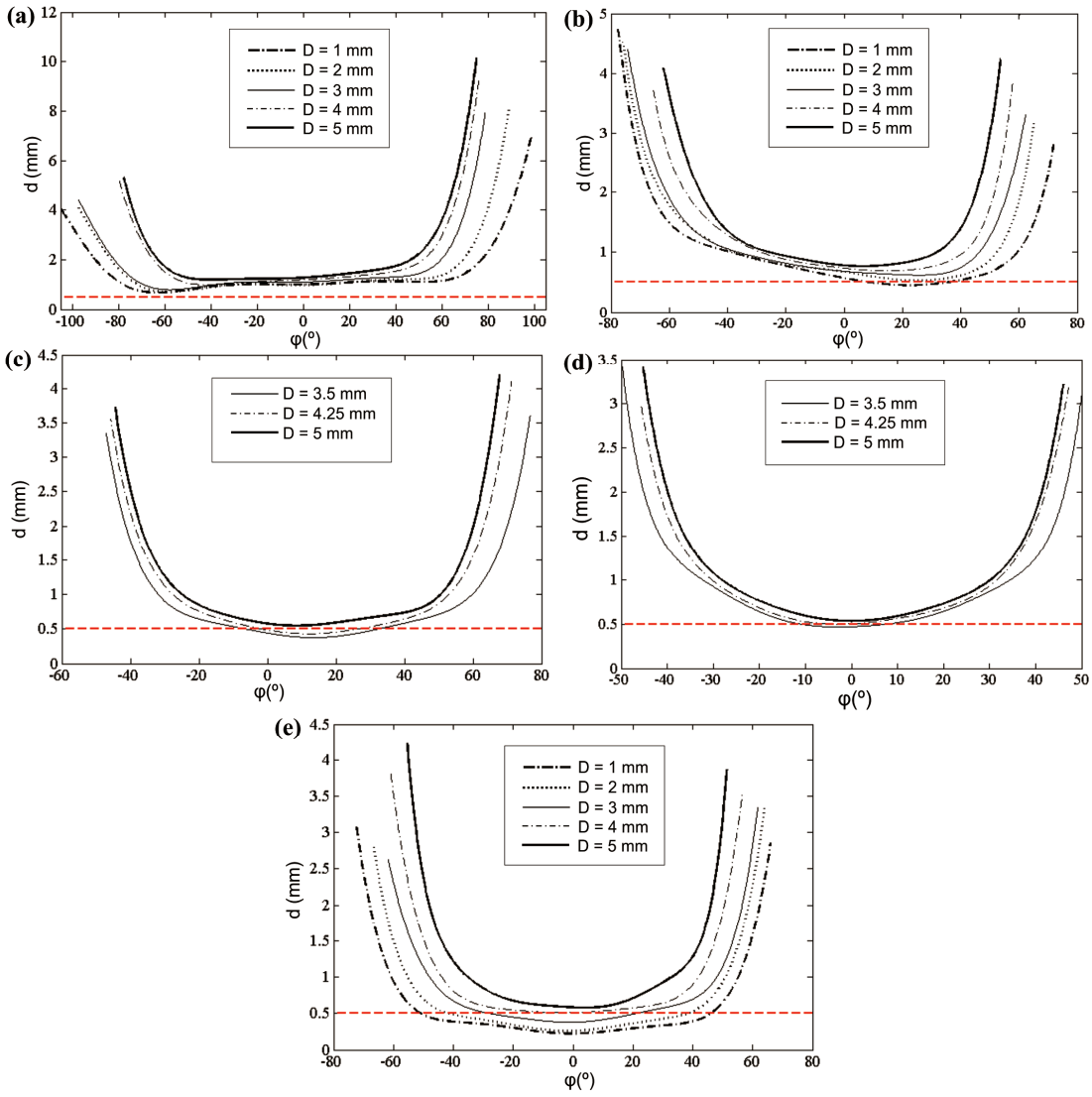

Figure 8 Distances obtained between the portal vein and the thermal lesion for different vessel-device distances (D), device-tissue contact conditions, and relative position of the vessel. Cases (see Fig. 7 for more details): total vessel-device contact and vessel perpendicular below the center of the device **(a)**, below its proximal end **(b)** and below its distal end **(c)**, vessel parallel to the device **(d)**, and only proximal vessel-device contact and vessel perpendicular to the device **(e)**. The horizontal dashed line represents the vessel wall thickness (0.5 mm).

Figure 7(a) shows the thermal lesions created with total device-tissue contact and the portal vein perpendicular to the device at different distances (D from 1 to 5 mm) below its center. In this case the thermal lesion shape was modified by the heat sink effect

inside the vessel, i.e. the flowing blood provided a thermal protective effect, regardless of the vessel-device distance (see XZ-plane). As can be seen in Figure 8(a), the vessel wall was not damaged by the thermal lesion contour ($\Omega = 1$) after RF heating for all the vessel-device distances considered.

Figure 7(b) shows the thermal lesions created with total device-tissue contact and the portal vein perpendicular to the device at different distances (D from 1 to 5 mm) below its proximal end (i.e. where the electrode elbow is located). In this case the lesion shape was significantly modified around the vessel for all vessel-device distances (see XZ-plane), although 7.26% of the vessel wall was damaged (which corresponds to $\beta = 26.15º$) at D = 1 mm, as shown in Figure 8(b).

Figure 7(c) shows the thermal lesions created with total device-tissue contact and the portal vein perpendicular to the device at different distances (D from 3.5 to 5 mm) below its distal end (i.e. where the blade is located). As before, thermal lesion shape was significantly modified by the heat sink effect caused by blood flow inside the vessel (see XZ-plane in Figure 7(c)). In this case the vessel wall was damaged at $D \leq 4.25$ mm, as shown in Figure 8(c): 12.7% and 6.7% (with β of 43.8º and 24.12º) at D = 3.5 and 4.25 mm, respectively.

Figure 7(d) shows the thermal lesions created with total device-tissue contact and the portal vein parallel to the device at different distances (D from 3.5 to 5 mm) below it. As can be observed in Figure 7(d) on the YZ-plane, the thermal lesion shape around the vessel was also modified by the heat sink effect for all vessel-device distances (D). In this case the vessel wall was damaged at $D \leq 4.25$ mm, as shown in Figure 8(d): 5.88% and 2.21% ($\beta = 21.17º$ and 7.94º) at D = 3.5 and 4.25 mm, respectively.

Figure 7(e) shows the thermal lesions created after RF heating for the case of only proximal device-tissue contact (elbow zone) and the portal vein perpendicular to the

device and at different distances (D from 1 to 5 mm) below its contact point. As expected, the thermal lesion is restricted to the area around the contact point, and hence is much smaller than the total contact cases. Although the thermal lesion shape was modified around the vessel for all vessel-device distances (see XZ-plane in Figure 7(e)), the vessel wall was damaged at $D \leq 4$ mm, as shown in see Figure 8(e). The damage to the vessel wall was 26.96%, 20.14%, 13.88% and 0.65% (β = 89.84º, 72.49º, 49.97º and 2.33º) when D was increased from 1 to 4 mm. However, when the blood flow was doubled (0.4 m s^{-1}), the vessel wall was protected up to $D \geq 4$ mm. This was the maximum distance for which the vessel was not damaged, even when the blood flow velocity was increased.

Table II shows the values of initial impedance (Z_i), initial power (P_i), delivered energy (E) and maximum temperature reached in the tissue (T_{max}) for the cases considered. Z_i was seen to be much greater (up to twice as high) for the case in which the proximal part of the device (elbow zone) was placed on the tissue than with complete contact. Z_i rose slightly when D was increased from 1 to 5 mm for all configurations: approximately $\approx 2\ \Omega$ in the case of total support and up to 15 Ω for proximal contact. In general, the higher the Z_i, the lower the P_i. Finally, T_{max} was slightly higher with only proximal contact (elbow zone), whereas E was half that of the total contact cases (approximately 2 kJ versus 1 kJ).

Table II. Initial impedance (Z_i), initial power (P_i), distributed energy (E), maximum temperature reached in the tissue (T_{max}) for the cases studied. D: distance between the RF device and the large vessel (portal vein).

Cases		$\mathbf{Z_i}$ **(Ω)**	$\mathbf{P_i}$ **(W)**	**E (kJ)**	$\mathbf{T_{max}}$ **(ºC)**
Device-tissue contact / vessel position with respect to the device	**D (mm)**				
Complete / perpendicular below its center	1	67.05	37.28	1.982	106.14
	2	67.98	36.78	1.980	109.17
	3	68.64	36.42	1.979	105.39
	4	69.00	36.23	1.980	107.07
	5	69.21	36.12	1.979	109.42
Complete / perpendicular below its proximal end	1	67.29	37.15	1.958	109.05
	2	68.36	36.57	1.964	107.73
	3	69.08	36.19	1.972	108.67
	4	69.59	35.93	1.970	107.67
	5	69.75	35.84	1.972	107.07
Complete / perpendicular below its distal end	3.5	69.09	36.18	1.966	108.22
	4.25	69.44	36.00	1.965	106.48
	5	69.69	35.87	1.968	108.13
Complete / parallel below it	3.5	66.16	37.78	2.016	106.37
	4.25	67.05	37.28	2.022	106.83
	5	67.86	36.84	2.019	108.49
Proximal (elbow) / perpendicular below its contact point	1	155.77	16.05	0.947	118.34
	2	161.82	15.45	0.970	113.23
	3	165.24	15.13	0.983	118.61
	4	167.70	14.91	0.985	112.86
	5	170.93	14.63	0.978	118.26

IV. DISCUSSION

The aim of this study was to assess whether the heat sink effect caused by the blood flow inside a large vessel (the portal vein) could thermally protect its wall during monopolar RF heating by an internally cooled electrode. As far as we know, this issue has not been explicitly addressed before, since previous studies focused exclusively on determining how the heat sink effect could distort coagulation shape during RF ablation.[19,22,31,35-38] Therefore, knowing the conditions under which the heat sink effect inside the vessel thermally protects its wall could be useful to physicians when making a preliminary assessment of vascular damage in their treatment plans.

In our study we used an in vivo experimental set-up, which obviously presents the problem of not having complete control of most of the variables (such as vessel-device distance, vessel wall thickness, blood flow inside the vessel, etc.) as compared to ex vivo or phantom-based models. Previous studies[39,40] used an ex vivo experimental approach in which the vessels were simulated by glass tubes and the blood flow by means of a saline flow controlled by a roller pump. However, we consider that the electrical insulation characteristics of the glass tube near the RF electrode could alter the electric field, so that this *insulating vessel* could be used to study temperature distributions and thermal lesions, as long as the vessel is placed sufficiently far away from the RF device. In order to demonstrate this we conducted an additional computer simulation (device in total contact with the tissue and vessel perpendicular to the device at a distance of 5 mm below its center) considering an electrical *insulating vessel*. We compared the thermal results in both situations (i.e. blood vessel vs. *insulating vessel*) and observed that the temperature distributions and thermal lesions were different near the vessel, as shown in Figure 9. The temperatures in the center of the tissue below the device were around 70ºC and 50ºC with blood and *insulating* vessel, respectively. We

therefore concluded that conducting an ex vivo study with a glass vessel (as portal vein) would not be suitable in our case for modeling thermal lesion dimensions in the proximity of the vessel.

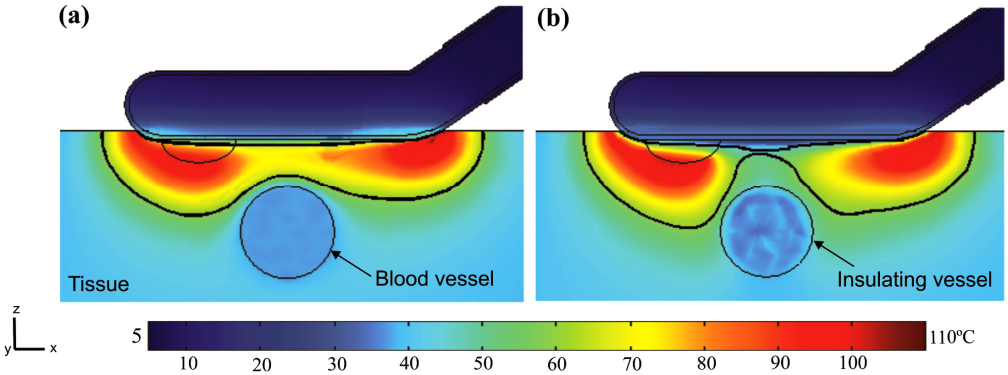

Figure 9 Temperature distributions (in ºC) around the portal vein after 45 s of RF heating, considering the device in total contact with the tissue and the portal vein perpendicular to the device and at a distance (D) of 5 mm below its center. The portal vein was considered as **(a)** a blood vessel, and **(b)** an *insulating vessel*. The solid black line is the thermal damage border ($\Omega = 1$).

Our in vivo experimental study was conducted in order to assess the ability of the computational model to predict the shapes of thermal lesions created around a vessel by the RF-based device considered. Although the computational modeling study was planned for large vessels (such as the portal vein) close to the RF device, in the experiments we did not find any vessels situated at a distance less than 5 mm from the RF device with a diameter greater than 7.6 mm. We simulated all the experimental cases and verified the agreement between the thermal lesion geometries from the computational and experimental results (see Figure 5(b)-(c)). No damaged vessel wall was found. These results suggest that the computer model could be a useful tool for assessing situations for which no experimental results are available, e.g. in which the vessel has a larger diameter (such as the portal vein, in our case) and is located closer to the RF-assisted device.

The computational results showed an evolution of the temperature distributions during RF-assisted resection characterized by the preferential heating of the tissue located under the edges of the device (tip of the blade and at proximal edge) (see Figure 6). The middle zone was heated mainly by thermal conduction from these zones. The reason for this is the well-known edge effect, which is based on the high electrical gradient at these points which causes considerable Joule heating, resulting in a marked temperature increase. The existence of the edge effect in these zones will unquestionably affect the possibility of thermal damage to a vessel close to such zones.

The computer results also showed that the thermal lesion shape was significantly modified by the heat sink effect inside the portal vein for most of the cases considered (see Figure 7). Only in the case of complete device-tissue contact and with the portal vein in the central zone of the electrode (see Figure 7(a)) did the vessel wall remain undamaged, even for a vessel-device distance of 1 mm (see Figure 8(a)). The explanation for this is precisely because this zone is not influenced by the edge effect described above. In other words, the tissue under the center of the device is heated to a lower temperature than the zone below the edges of the device (see Figure 6). The edge effect is boosted even further by the cooling effect of the blood inside the vessel (pushing the hottest point within the tissue).

In the cases involving complete device-tissue contact, vessel perpendicular to the electrode and with the vessel below the ends of the device, distal (blade zone) and proximal (elbow zone), the vessel wall was more seriously damaged than when the vessel was below the central zone of the device (see Figures 7(b) and (c)). Consequently, surgeons should take special care when the edges of the RF electrode, especially the blade tip, come into contact with a proximal vessel. In short, the computer results suggest that a minimum distance of 5 mm should be maintained between the RF-

assisted device and the portal vein, as it is not possible to completely ensure that the vessel will be positioned exactly at the center of the device (where shorter distances could be equally safe).

We also studied the effect of increasing the blood flow velocity inside the portal vein to assess its influence as a protective mechanism of the vessel wall from thermal damage. We considered the case of proximal contact between device and tissue, since it was one in which the vessel wall was damaged for greater vessel-device distances and there was no influence of the blade tip. Our computer results suggest that a higher flow velocity (0.4 m s^{-1}) could protect the vessel wall up to a maximum vessel-device distance of 4 mm. This means it is not possible to protect the vessel wall to shorter distances, even further increasing the blood flow velocity.

As shown in Table II, the initial impedance in the case of proximal contact was approximately twice as high as with total contact. This was due to the device-tissue contact area being much smaller, which implies higher current density. Although higher Z_i implied lower P_i (since RF power is inversely proportional to impedance and the voltage was constant) the maximum temperature was also greater in this case, due to the power being deposited in a much smaller volume than in the case with total contact. From a practical point of view, this result suggests that great care should be taken when there is a vessel near the electrode and the device-tissue contact area is small. This situation could also occur when only the blunt distal end of the electrode is used, e.g. when after removing a fragment of the organ the blunt tip is used to apply RF current on the remaining section surface in performing preventive coagulation to minimize postoperative bleeding and leaks.

The effect of vessel-device distance on initial impedance was almost negligible. The drop in impedance at shorter distances was due to the electrical conductivity of the

blood (0.667 S/m) being higher than that of the tissue (0.33 S/m). However, the influence of the tissue between the device and the vessel may account for the negligible influence of the vessel on initial impedance. This suggests that a predictive method of assessing the proximity of a large vessel by measuring impedance would not be feasible.

Even though there are no previous studies on the effect of an RF-based surgical device in the proximity of a large vessel, some other experimental results could also be compared to our computer results. For instance, Ng *et al.*[41] studied the local effect of RF ablation with a 3-mm electrode Cool-Tip on the left main portal vein. They found that RF ablation was safe at 5 mm from the main portal vein branch. The same study indicates the importance of blood flow for the thermal protection of the vessel, since the use of a Pringle maneuver (i.e. stopping internal blood flow) caused damage to the vessel wall. On the other hand, in another experimental study on RF ablation (50 W power) adjacent to large hepatic veins, some cases of intimal damage to large veins were reported when the electrode tips were within 5 mm of the confluence of the hepatic veins.[42] A third experimental study on RF ablation with a Starburst XL electrode reported that when the electrode was placed 10 mm (±1 mm) away from the portal vein, the delivered power was not able to overcome the heat dissipated by the vein, so that the coagulation zones around the vessels were distorted.[43] These experimental findings suggest that the threshold value for the distance between an RF heating electrode and large hepatic vessels should be around 5 mm if thermal damage to the vessel wall is to be avoided, which is in close agreement with the value suggested by our computer results.

Limitations of the study

The developed computational modeling was used to study the effect of different relative positions and distances between the portal vein and the RF-based device on the potential thermal damage to the vessel wall. The model thus does not allow predictions to be made as to the thermal injury risk in absolute terms, since a partially damaged vessel wall could imply a significant clinical problem (such as vascular thrombosis). This issue is obviously outside the scope of a computer modeling study. Moreover, individual variations and the anatomical complexity of the liver tissue to be transected could have a considerable effect on the final phenomena, e.g. several vessels (arteries and veins) could be present in the transection line. Another limitation is that we only considered the case of the portal vein. The results could be dissimilar for other vessels (e.g. hepatic vein) with different flow rates.[44] Since we did not compare the thermal lesions in the depth direction of the computer-simulated results with those of the experiments, it would be valuable to further conduct in vivo animal studies or human clinical studies to validate the simulated thermal lesions around the blood vessel in 3D and the minimum safe vessel-device distance obtained by the proposed computer model.

V. CONCLUSIONS

The geometries of the thermal lesions around the vessels in the in vivo experiments were in agreement with the computer results. The thermal lesion shape created around the portal vein was significantly modified by the heat sink effect in all the cases considered. Thermal damage to the portal vein wall was inversely related to the vessel-device distance. It was also more pronounced when the device-tissue contact surface was reduced (proximal contact) or when the vessel was parallel to the device or perpendicular to its distal end (blade zone), the vessel wall being damaged at distances

shorter than 4.25 mm. Consequently, under the simulated conditions, the computational findings suggest that the heat sink effect could protect the portal vein wall for distances equal to or longer than 5 mm, regardless of its position and distance with respect to the RF-based device.

ACKNOWLEDGEMENTS

This work received financial support from the Spanish "Plan Nacional de I+D+I del Ministerio de Ciencia e Innovación" Grant No. TEC2011-27133-C02-01 and -02, also from the Universitat Politècnica de València (INNOVA11-01-5502; and PAID-06-11 Ref. 1988). A. González-Suárez is the recipient of a Grant VALi+d (ACIF/2011/194) from the Generalitat Valenciana.

DISCLOSURE STATEMENT

E.B and F.B. declare a stock ownership in Apeiron Medical S.L. This company has a license for Patent US 8.303.584, on which the device considered in this study is based. The remaining authors have no conflict of interest or financial ties to disclose.

References

[1] R.T. Poon, S.T. Fan and J. Wong, "Liver resection using a saline-linked radiofrequency dissecting sealer for transection of the liver," J. Am. Coll. Surg. **200**(2), 308-313 (2005).

[2] F. Burdío, L. Grande, E. Berjano, M. Martinez-Serrano, I. Poves, J.M. Burdío, A. Navarro and A. Güemes, "A new single-instrument technique for parenchyma division and hemostasis in liver resection: a clinical feasibility study," Am. J. Surg. **200**(6), e75-80 (2010).

[3] S.A. Topp, M. McClurken, D. Lipson, G.A. Upadhya, J.H. Ritter, D. Linehan and S.M. Strasberg, "Saline-linked surface radiofrequency ablation: factors affecting steam popping and depth of injury in the pig liver," Ann. Surg. **239**(4), 518-527 (2004).

[4] K. Tepetes, "Risks of the radiofrequency-assisted liver resection," J. Surg. Oncol. **97**(2):193 (2008).

[5] F. Marchal, D. Elias, P. Rauch, R. Zarnegar, A. Leroux, J.L. Verhaeghe, F. Guillemin, J.P. Carteaux, J.P. Villemont, "Prevention of biliary lesions that may occur during radiofrequency ablation of the liver: study on the pig," Ann. Surg. **243** (1), 82-88 (2006).

[6] P.A. Sutton, S. Awad, A.C. Perkins and D.N. Lobo, "Comparison of lateral thermal spread using monopolar and bipolar diathermy, the Harmonic Scalpel and the Ligasure," Br. J. Surg. **97**(3), 428-433 (2010).

[7] J.M. Lee, J.K. Han, J.M. Chang, S.Y. Chung, S.H. Kim, J.Y. Lee, M.W. Lee and B.I. Choi, "Radiofrequency ablation of the porcine liver in vivo: increased coagulation with an internally cooled perfusion electrode," Acad. Radiol. **13**(3), 343-352 (2006).

[8] S.N. Goldberg, C.J. Grassi, J.F. Cardella, J.W. Charboneau, G.D. Dodd 3rd, D.E. Dupuy, D. Gervais, A.R. Gillams, R.A. Kane, F.T. Lee Jr, T. Livraghi, J. McGahan, D.A. Phillips, H. Rhim and S.G. Silverman. Society of Interventional Radiology Technology Assessment Committee; International Working Group on Image-Guided Tumor Ablation, "Image-guided tumor ablation: Standardization of terminology and reporting criteria," Radiology **235**(3), 728-739 (2005).

[9] H.H. Pennes, "Analysis of tissue and arterial blood temperatures in the resting human forearm," J Appl. Physiol. **1**(2), 93-122 (1948).

[10] J.P. Abraham and E.M. Sparrow, "A thermal-ablation bioheat model including liquid-to-vapor phase change, pressure- and necrosis-dependent perfusion, and moisture-dependent properties," Int. J. Heat Mass. Tran. **50**(13-14), 2537-2544 (2007).

[11] J. Byeongman and A. Alptekin, "Prediction of the extent of thermal damage in the cornea during conductive keratoplasty," J. Therm. Biol. **35**(4), 167-174 (2010).

[12] E.J. Berjano, "Theoretical modeling of epicardial radiofrequency ablation: state-of-the-art and challenges for the future," Biomed. Eng. Online **5**:24 (2006).

[13] G. Zhao, H.F. Zhang, X.J. Guo, D.W. Luo and DY Gao, "Effect of blood flow and metabolism on multidimensional heat transfer during cryosurgery," Med. Eng. Phys. **29**, 205-215 (2007).

[14] T. Pätz, T. Körger and T. Preusser, "Simulation of Radiofrequency Ablation Including Water Evaporation," presented at the World Congress on Medical Physics and Biomedical Engineering, Munich, Germany, September 7-12, 2009.

[15] I. Chang and U. Nguyen, "Thermal modelling of lesion growth with radiofrequency ablation devices," Biomed. Eng. Online **3**(1):27 (2004).

[16] I.A. Chang, "Considerations for thermal injury analysis for RF ablation devices," Open Biomed. Eng. J. **4**, 3-12 (2010).

[17] S. Tungjitkusolmun, S.T. Staelin, D. Haemmerich, J.Z. Tsai, J.G. Webster, F.T. Lee Jr, D.M. Mahvi and V.R. Vorperian, "Three-Dimensional finite-element analyses for radio-frequency hepatic tumor ablation," IEEE Trans. Biomed. Eng. **49**(1), 3-9 (2002).

[18] S. Jacques, S. Rastegar, S. Thomsen and M. Motamedi, "Nonlinear finite-element analysis of the role of dynamic changes in blood perfusion and optical properties in laser coagulation of tissue," IEEE J. Sel. Top Quantum Electron. **2**, 922-933 (1996).

[19] C.L. Antunes, T.R. Almeida and N. Raposeiro, "Saline-enhanced RF ablation on a cholangiocarcinoma: a numerical simulation," COMPEL: The International Journal for Computational and Mathematics in Electrical and Electronic Engineering **31**, 1050-1066 (2012).

[20] F.P. Incropera, D.P. DeWitt, T.L. Bergman and A.S. Lavine, *Fundaments of Heat and Mass Transfer*, 6th ed. (John Wiley & Sons, Inc., Hoboken, 2006).

[21] J.D. Doss, "Calculation of electric fields in conductive media," Med. Phys. **9**(4), 566-573 (1982).

[22] D. Haemmerich, A.W Wright, D.M. Mahvi, F.T. Lee Jr and J.G. Webster, "Hepatic bipolar radiofrequency ablation creates coagulation zones close to blood vessels: a finite element study," Med. Biol. Eng. Comput. **41**(3), 317-323 (2003).

[23] E.J. Berjano, F. Burdío, A.C. Navarro, J.M. Burdío, A. Güemes, O. Aldana, P. Ros, R. Sousa, R. Lozano, E. Tejero and M.A. Gregorio, "Improved perfusion system for bipolar radiofrequency ablation of liver," Physiol. Meas. **27**(10), 55-66 (2006).

[24] F. Duck, Physical properties of tissue - A comprehensive reference book (Academic Press, New York, 1990).

[25] F. Burdío, E.J. Berjano, A. Navarro, J.M. Burdío, L. Grande, A. Gonzalez, I. Cruz, A. Güemes, R. Sousa, J. Subirá, T. Castiella, I. Poves and J.L. Lequerica, "Research and development of a new RF-assisted device for bloodless rapid transection of the liver: Computational modeling and in vivo experiments," Biomed. Eng. Online **8**:6 (2009).

[26] J. Pearce, D. Panescu and S. Thomsen, "Simulation of diopter changes in radio frequency conductive keratoplasy in the cornea," WIT Trans. Biomed. Health **8**, 469-477 (2005).

[27] D. Haemmerich, L. Chachati, A.S. Wright, D.M. Mahvi, F.T. Lee, JG. Webster, "Hepatic radiofrequency ablation with internally cooled probes: effect of coolant temperature on lesion size," IEEE Trans. Biomed. Eng. **50**, 493–499 (2003).

[28] E. Berjano and A. d'Avila, "Lumped element electrical model based on three resistors for electrical impedance in radiofrequency cardiac ablation: estimations from analytical calculations and clinical data," Open Biomed. Eng. J. **7**, 62-70 (2013).

[29] S. Gray, *Gray's Anatomy* (Vintage Books, New York, 1990).

[30] P.H. Hannesson, H. Stridbeck, C. Lundstedt, A. Andrén-Sandberg and I. Ihse, "Intravascular ultrasound of the portal vein—normal anatomy," Acta Radiol. **36**(4), 388-392 (1995).

[31] X. Chen and G.M. Saidel, "Mathematical modeling of thermal ablation in tissue surrounding a large vessel," J. Biomech. Eng. **131**(1), 011001 (2009).

[32] T. Peng, D. O'Neill and S. Payne, "Mathematical study of the effects of different intrahepatic cooling on thermal ablation zones," presented at the 33rd Annual International Conference of the IEEE Eng. Med. Biol Soc., Boston, August 30-September 3, 2011.

[33] J.L. Cioni, P. D'Alimonte, A. Cristani, P. Ventura, G. Abbati, E. Tincani, R. Romagnoli and E. Ventura, "Duplex-Doppler assessment of cirrhosis in patients with chronic compensated liver disease," J. Gastroenterol. Hepatol. **7**(4), 382-384 (1992).

[34] J.S. Ríos, J.M. Zalabardo, F. Burdio, E. Berjano, M. Moros, A. Gonzalez, A. Navarro and A. Güemes, "Single instrument for hemostatic control in laparoscopic partial nephrectomy in a porcine model without renal vascular clamping," J. Endourol. **25**(6), 1005-1011 (2011).

[35] I. Dos Santos, D. Haemmerich, S. Pinheiro Cda and A.F. da Rocha, "Effect of variable heat transfer coefficient on tissue temperature next to a large vessel during radiofrequency tumor ablation," Biomed. Eng. Online **7**:21 (2008).

[36] L. Consiglieri, I. Dos Santos and D. Haemmerich, "Theoretical analysis of the heat convection coefficient in large vessels and the significance for thermal ablative therapies," Phys. Med. Biol. **48**, 4125-4134 (2003).

[37] L. Consiglieri, "Continuum models for the cooling effect of blood flow on thermal ablation techniques," Int. J. Thermophys. **33**, 864-884 (2012).

[38] H.W. Huang, "Influence of blood vessel on the thermal lesion formation during radiofrequency ablation for liver tumors," Med Phys. **40**(7), 073303 (2013).

[39] C. Welp, S. Siebers, H. Ermert, J. Werner, "Investigation of the influence of blood flow rate on large vessel cooling in hepatic radiofrequency ablation," Biomed. Tech. (Berl). **1**(5-6), 337-346 (2006).

[40] K.S. Lehmann, J.P. Ritz, S. Valdeig, V. Knappe, A. Schenk, A. Weihusen, C. Rieder, C. Holmer, U. Zurbuchen, P. Hoffmann, H.O. Peitgen, H.J. Buhr and B.B. Frericks, "Ex situ quantification of the cooling effect of liver vessels on radiofrequency ablation," Langenbecks Arch. Surg. **394**(3), 475-481 (2009).

[41] K.K. Ng, C.M. Lam, R.T. Poon, T.W. Shek, S.T. Fan and J. Wong, "Delayed portal vein thrombosis after experimental radiofrequency ablation near the main portal vein," Br. J. Surg. **91**(5), 632-639 (2004).

[42] M.S. Metcalfe, E.J. Mullin, M. Texler, D.P. Berry, A.R. Dennison and G.J. Maddern, "The safety and efficacy of radiofrequency and electrolytic ablation created adjacent to large hepatic veins in a porcine model," Eur. J. Surg. Oncol. **33**(5), 662-667 (2007).

[43] C. Bangard, A. Gossmann, H.U. Kasper, M. Hellmich, J.H. Fischer, A. Hölscher, K. Lackner and D.L. Stippel, "Experimental radiofrequency ablation near the portal and the hepatic veins in pigs: differences in efficacy of a monopolar ablation system," J. Surg. Res. **135**(1), 113-119 (2006).

[44] T. Kröger, T. Preusser and H.O. Peitgen, "Blood Flow Induced Cooling Effect in Radio Frequency Ablation for Hepatic Carcinoma," IPAM UCLA May 19–23, 2008.